Submitted to *Nature Communications*

Orbital forcing of ice sheets during snowball Earth

Ross N. Mitchell[1,2], Thomas M. Gernon[3†], Grant M. Cox[2], Adam R. Nordsvan[2,4], Uwe Kirscher[2,5], Chuang Xuan[3], Yebo Liu[2], Xu Liu[1] & Xiaofang He[6]

[1] State Key Laboratory of Lithospheric Evolution, Institute of Geology and Geophysics, Chinese Academy of Sciences, Beijing 100029, China

[2] Earth Dynamics Research Group, The Institute for Geoscience Research (TIGeR), Department of Earth and Planetary Sciences, Curtin University, GPO Box U1987, Perth WA 6845, Australia.

[3] School of Ocean and Earth Science, University of Southampton, Southampton, SO22 4JR, UK.

[4] Department of Earth Sciences, University of Hong Kong, Pokfulam, Hong Kong, China.

[5] Department of Geosciences, Eberhard Karls University Tübingen, Sigwartstr. 10, Tübingen 72076, Germany.

[6]School of Geoscience and Survey Engineering, China University of Mining and Technology (Beijing), Beijing 100083, China.

These authors contributed equally: R.N.M. and T.M.G.

ABSTRACT

The snowball Earth hypothesis—that a runaway ice-albedo feedback can cause global glaciation—seeks to explain low-latitude glacial deposits, as well as geological anomalies including the re-emergence of banded iron formation and "cap" carbonates. One of the most significant challenges to

snowball Earth has been sedimentological cyclicity that has been taken to imply more climate dynamics than expected when the ocean is completely covered in ice. However, recent climate models suggest that as atmospheric CO_2 accumulates, the snowball climate system becomes sensitive to orbital forcing. Here we show the presence of nearly all Milankovitch (orbital) cycles preserved in stratified banded iron formation deposited during the Sturtian snowball Earth. These results provide evidence for orbitally forced cyclicity of global ice sheets that resulted in periodic oxidation of ferrous iron. Orbital glacial advance and retreat cycles provide a simple mechanism to reconcile both the sedimentary dynamics and the enigmatic survival of multicellular life during snowball Earth.

INTRODUCTION

Astronomical "Milankovitch" cycles[1], related to changes in Earth's orbit around the sun, exert a fundamental control on climate variability over tens to hundreds of thousands of years (kyr), with modulations in hundreds of kyr and even millions of years (Myr). Orbital forcing has presumably operated throughout Earth history with evidence found as old as ca. 2480 Myr ago[1-4], and may have influenced the course of severe "snowball Earth" glaciations[5,6], notably during the Cryogenian Period, about 720 to 635 Myr ago. Under snowball conditions, astronomical-induced variations in insolation due to Earth's precession, obliquity, and eccentricity should be ongoing, but the range of associated climate variability and mechanisms in an ice-covered ocean are poorly understood. Recent ice sheet and atmospheric modeling results indicate that orbital forcing should be a viable climate driver under a wide

range of atmospheric concentrations of CO_2 between 0.1 and 200 mbar, and therefore was likely to have modulated ice sheet volume throughout much of the Cryogenian Period[5].

While evidence for orbital forcing has been suggested in Cryogenian glacial successions[5], evidence for multiple, internally consistent timescales of orbital forcing has not been demonstrated. This is likely because most glacial deposition occurs irregularly[7], forming glacial diamictites (that is, lithified sediments comprising chaotic mixtures of a wide range of clast- and grain-size distribution) only rarely preserving stratification. One notable exception is the deglacial succession of the Elatina Formation with its tidal rhythmites[8]. Cyclostratigraphy—the study of orbital forcing in sedimentary successions—usually operates under the assumption of constant sediment accumulation (e.g., as expected in pelagic and hemi-pelagic facies[1]), so its application is hindered in sequences that do not preserve stratification (e.g., diamictite) or are characterized by frequent and abrupt changes in sediment accumulation rates (e.g., as in a delta front).

Here we show that banded iron formation (BIF)[9,10]—well-stratified sedimentary rock containing abundant iron oxide—is ideally suited to cyclostratigraphic analysis because it is closely associated with glacial diamictites[9-12], and deposited at a relatively constant rate when averaged over multiple depositional cycles as evidenced by the rhythmic banding[13,14] on decimetre and centimetre (Fig. 1d; Supplementary Fig. 1d) and millimetre scales (Supplementary Fig. 2). Precambrian BIF has also been demonstrated to be both susceptible to orbital forcing and amenable to recording a clear orbital signal[4].

The occurrence of BIF in Neoproterozoic glacial deposits was initially conceived as a "last gasp" for global glaciation[15] and thought to represent oxidation of hydrothermal iron accumulated within a snowball ocean after the re-emergence of open ocean conditions[6,15]. However, this concept cannot readily explain how BIF in some cases is overlain or interbedded with glacial diamictites[11]. Most recently, BIF deposited during snowball Earth have been interpreted as the product of hydrothermally-derived iron mixing with oxidized subglacial meltwater[16].

RESULTS

Stratigraphy and magnetic susceptibility

We studied BIF sequences and their associated glacial deposits[11] from the Sturtian glaciation in the Flinders Ranges of South Australia (Fig. 1; Supplementary Fig. 3). We performed time series analysis (Methods) that requires both adequate sampling resolution to detect high-frequency (short-wavelength) signals and long records for detecting low-frequency (long-wavelength) signals. To satisfy these requirements, we sampled Oraparinna Station (Figs. 1b and 2 and Supplementary Figs. 3-6; Supplementary Table 1) at 1-metre (m) intervals, allowing us to capture cycles with periods of several metres. A stratigraphic section at Holowilena, approximately 75 km south of Oraparinna (Fig. 1b; Supplementary Fig. 3), provided continuous exposure over a shorter interval and was sampled at 25 cm intervals to determine cycles with periods > 50 cm (Fig. 1b and Supplementary Figs. 3 and 7; Supplementary Table 2). Therefore, our sampling at Holowilena targeted high-frequency Milankovitch cycles (precession, obliquity, and short eccentricity) and at Oraparinna targeted low-frequency

Milankovitch modulations (long eccentricity as well as ~1.2-Myr and ~2.4-Myr modulations of obliquity and eccentricity, respectively). This sampling strategy was designed around the outcrop conditions, where the river cut bank at Holowilena provides complete exposure over a short stratigraphic interval and the mountainside draw (or re-entrant) at Oraparinna provides incomplete but relatively consistent exposure over the entire BIF stratigraphy. The overall thicknesses and the lithofacies of the Holowilena BIF at both sections are strikingly comparable and nearly identical[10]. Given the proximity of Holowilena and Oraparinna and their near-matching stratigraphies, and that the eccentricity band spans target cycles at both localities, matching their short and long eccentricity are expected to yield comparable sediment accumulation rates. Faulting occurs ~1 km away from the Holowilena section[17]; nonetheless, we can confirm that the contact between the Holowilena BIF and the underlying Pualco Tillite is not faulted (Supplementary Fig. 3) and no significant faults were observed during detailed mapping of the ~18-m-thick section at Holowilena Creek, either in this study or in earlier investigations[10,11].

Magnetic susceptibility—the measure of magnetizable minerals in a rock layer—was used as our cyclostratigraphic proxy for the BIF (Methods; Supplementary Fig. 8). Magnetic susceptibility is one of the more successful proxies used in astrochronology[18], and our utilization is also motivated by our rock magnetic experiments, which indicate that the Holowilena BIF is highly variable in its hematite and magnetite content (Methods). Cyclostratigraphy has previously been applied to the Cryogenian interglacial (i.e., the ~10 Myr period between the Sturtian and Marinoan [~650–635 Myr ago] glaciations), yielding an astronomical interglacial chronology[2,19]. Cycles in magnetic susceptibility of

Cryogenian BIF, if present, could be the result of either orbital forcing (i.e., allocyclic) or more autocyclic processes (e.g., glacial surges related to ice dynamics producing an equivalent sedimentary response). Therefore, it is critical to conduct rigorous time series analysis (Methods).

Time series analysis

Our magnetic susceptibility data exhibit multiple statistically significant cycles at both sites (Fig. 3). At Holowilena, two cycles (periods of ~4 m and ~1 m) rise above the 95% confidence level (Fig. 3a and b). At Oraparinna, three cycles (periods of ~18 m, ~32 m, and ~53 m) rise above the 95% confidence level (Fig. 3c and d). The five bands identified (Fig. 3) can be compared with target astronomical cycles of Neoproterozoic age (Supplementary Fig. 9) by assuming a sediment accumulation rate (Supplementary Table 3). Beyond our measured section, the synglacial Sturtian stratigraphy at Oraparinna is complicated by local tectonics and salt diapirism[20], so a regional sediment accumulation rate is inferred from the stratigraphic thicknesses at Holowilena.

Here, the syn-glacial Yudnamutana Subgroup, comprising the Pualco Tillite, Holowilena Ironstone, and Wilyerpa Formation (Fig. 1c), ranges in thickness along strike from 2068 to 2470 m (ref. [21]). A high-precision zircon U-Pb age of 663.03 ± 0.11 Myr (2σ) was recently reported from a tuffaceous bed in this region (Copley, SA), roughly 80 m down sequence from the contact with the Wilyerpa Formation[22], where lithofacies associations are comparable to those at Holowilena[11]. Assuming the accepted Sturtian onset age of 717 Myr[22] and taking the well-constrained syn-glacial age of ~663 Myr for this area, we

assume a net sediment accumulation rate for the Yudnamutana Subgroup of 3.7 to 4.4 cm kyr^{-1}, a firm starting point for matching observed cycles to putative matches with astronomical cycles. Using this range as an initial guide, we selected the rate for each stratigraphic section that minimizes the net misfit between all observed cycles and their respective targets cycles. We found that sediment accumulation rates inferred for both BIF sections, when matching observed cycles to astronomical targets (~4.2 cm kyr^{-1}; Supplementary Table 3), are self-consistent and within the plausible range of sediment accumulation rates for the Yudnamutana Subgroup. Intervals of stratified diamictite at Oraparinna (Fig. 2) appear to exhibit similar relatively constant sediment accumulation rates (Fig. 3d).

At Holowilena, the shortest cycle identified (~1 m) yields an inferred ~23 kyr period consistent with orbital precession, the highest-frequency astronomical cycle. The longest cycles detected at Holowilena are in the ~100 kyr band: (i) amplitude modulation of the presumed precession signal yields an envelope reminiscent of short ~95-125 kyr eccentricity (see below), and (ii) a narrow and unmodulated cycle at ~97 kyr that most likely represents the strong 95-kyr component of the 4-component short eccentricity signal. At Oraparinna, the shortest cycle represents ~405 kyr long eccentricity, Earth's "metronome"[23], considered the most stable astronomical period through time[1,24]. Thus, the short eccentricity signal is identified in the high-resolution section and long eccentricity is identified in the longer section, providing an overlap of the results in the eccentricity bandwidth. The longest, high-confidence cycle identified at Oraparinna (53 m) translates to a period of ~1.2 Myr, close to that of the long-term, modulation of obliquity[1] or the ~1 Myr modulation of precession[25]. Additionally, amplitude modulation

of the presumed long eccentricity signal of Oraparinna yields an envelope with a period of ~2.5 Myr, close to the ~2.4 Myr modulation of eccentricity[1]. The ratios of the cycles identified at the two sections of Holowilena BIF are thus internally consistent with each other when interpreted as the hierarchy of all known Milankovitch cycles and modulations (Fig. 3). The exclusive absence of a high-frequency obliquity signal at ~30 kyr could be explained by Australia's low palaeolatitude during deposition of the Holowilena BIF (Fig. 1a).

The magnetic susceptibility data from Holowilena pass one of the most diagnostic tests for orbital forcing: eccentricity extracted from precession. Due to its effect on Earth's equinoxes, eccentricity primarily affects insolation due to its amplitude modulation of precession[1,26]. Thus, in Phanerozoic cyclostratigraphy, the eccentricity signal is usually extracted from that of precession[1]. Using the Hilbert transform for the extraction (Methods), the envelope of the putative precession signal (~23 kyr) is systematically amplitude-modulated in bundles of ~5 cycles, consistent with precession modulated by eccentricity (Fig. 3b). Spectral analysis of the ~23 kyr Hilbert transform yields power in the short eccentricity band (Fig. 4), confirming that an eccentricity signal can be extracted from precession.

It should be noted that with ~5 precession cycles per short eccentricity cycle (Figs. 3b and 4), our results for the middle of the Sturtian glaciation imply anomalously slow precession compared to astronomical models[27-29] that estimate ~6.5 precession cycles per short eccentricity cycle at this age. There are several possible explanations to consider. Firstly, it is possible that available astronomical models[27,28], although

generally in agreement with each other, are inaccurate by this age. However, cyclostratigraphic data as old as 1.4 Gyr ago appear to support the long-term astronomical model trajectories[29]. Secondly, it is possible that missing precession cycles per short eccentricity cycle in minor unconformities or cyclic changes in sedimentation rate related to precession amplitude may distort the observed ratio with eccentricity. However, there are no unconformities in either of the studied sections and the strong evidence of eccentricity-modulated precession suggests that we have resolved the relative ratio of eccentricity and precession at this age. Ruling out problems with either the models or the data, we offer a third, albeit more speculative, option. It is feasible that this anomaly is related to the conversion of large volumes of seawater into extremely thick sea ice and continental ice sheets during the Cryogenian. Such a transfer of mass away from Earth's spin axis would reduce the moment of inertia and, in order to conserve angular momentum, have temporarily slowed Earth's rate of rotation. As precession is related to rotation rate but eccentricity is not, this mechanism might explain the unexpected bundling observed by us for this age. Then, upon snowball deglaciation, Earth's rotation would have resumed its previously fast rate of rotation. Importantly, such an effect on rotation has been modeled for Pleistocene glaciations[30] and would presumably have been much more substantial on snowball Earth. Garnering corroborating evidence and testing such a possibility with modeling is beyond the scope of this study and warrants further investigation.

In summary, we find that the origin of magnetic susceptibility cycles in the Holowilena Ironstone (Fig. 3) are best explained by orbital forcing based on (i) the close matches with all Milankovitch cycles and

modulations when assuming sediment accumulation rates constrained by independent geochronology; (ii) the reasonable and consistent implied sediment accumulation rates; and (iii) the striking evidence for eccentricity-modulated precession. If cycles in magnetic susceptibility in the Holowilena BIF were not orbital but autocyclic in origin, all observations would have to be regarded as coincidental.

DISCUSSION

Assuming orbital forcing controls variability in magnetic susceptibility in the BIF, the question then becomes by what mechanism the signal is recorded. Rock magnetic experiments of our ironstone samples (Methods) demonstrate that magnetic susceptibility varies due to Fe-oxide mineralogy, specifically, the relative proportions of hematite and magnetite. For a sample that yields one of the highest susceptibility values at Oraparinna (~71 m; Fig. 2), thermal magnetic experiments suggest that the magnetic phase comprises almost purely hematite with minor magnetite (Fig. 5; Supplementary Fig. 10). This result is surprising as the susceptibility of magnetite is two orders of magnitudes stronger than that of hematite, implying a dominance of hematite in the Holowilena Ironstone. Fe-oxide mineralogy varies more over the ~15 m stratigraphic interval than it does over the ~5 m interval (Fig. 2; Fig. 5a), consistent with variability in susceptibility driven predominantly by long (405 kyr) and short (~100 kyr) eccentricity cycles, respectively (Fig. 3). Samples collected at the base and the top of the Holowilena section that exhibits an upsection increase in susceptibility (Supplementary Fig. 8) yield magnetite- and hematite-dominated thermal susceptibility signatures, respectively (Fig. 5b). This confirms that susceptibility in the Holowilena BIF is dominantly controlled by pure (high susceptibility) or

200 subordinate (low susceptibility) proportions of hematite, just as we observed at Oraparinna (Fig. 5a).
201 Samples in which magnetite dominates, consistent with petrographic observations (Supplementary Fig.
202 2), exhibit irreversible thermal susceptibility experiments (BIF0100 and BIF006 in Figure 5), suggesting
203 the presence of clays that convert to magnetite upon cooling[31]; as clays are paramagnetic and would
204 contribute little to susceptibility compared with ferromagnetic minerals, their presence in such samples
205 is consistent with the observation that hematite-poor and magnetite-rich lithologies have low
206 susceptibility.
207
208 Hematite in the Holowilena BIF is interpreted as the product of the oxidation of dissolved Fe^{2+} due to
209 free O_2 (ref. [13]). Detailed petrography of a high susceptibility, hematite-pure sample from Holowilena
210 (HOL-1) reveals pore-filling euhedral hematite laths that suggest the hematite is authigenic and
211 precipitated out of the snowball ocean due to oxidation (Fig. 6). Two possible sources of oxygen must be
212 considered. According to a "hard" snowball scenario where temperatures are so low that surface melting
213 is absent and ablation is controlled by sublimation[12], a viable mechanism for orbitally paced oxygenation
214 of a snowball ocean would be meltwater injection when an ice sheet margin reached tidewater during
215 times of ice advance. In this case, meltwater discharge occurs when the ice margin advances to the coast,
216 but not when it retreats inland[32]. Alternatively, according to a "soft" or more dynamic snowball scenario,
217 air-sea gas exchange would allow for the oxidation of the dissolved Fe^{2+} pool during periods of glacial
218 retreat if ice-free regions of sea ice (i.e., polynyas) open up[11]. These two models thus make testable,

219 opposite predictions, with oxygenation of the snowball ocean occurring during glacial advance
220 (tidewater model) and retreat (polynya model).
221
222 Depending on whether the hematite>magnetite (high magnetic susceptibility) phase of each orbital cycle
223 correlates with glacial advance or retreat can potentially test between the tidewater and polynya models
224 and their respective oxidizing agents (glacial meltwater and the atmosphere, respectively). In addition to
225 Fe-oxide mineralogy, magnetic susceptibility also varies consistently with δ^{56}Fe isotope variations[10] (Fig.
226 2), which are redox-sensitive and have been interpreted in terms of glacioeustasy[10] and subglacial
227 meltwater oxygenation[16]. The increase in δ^{56}Fe values in the lower-to-middle Holowilena BIF
228 corresponds with a sedimentological change from ice-proximal (diamictite/dropstone-dominated) to
229 ice-distal (mudstone with rare dropstones) facies (Fig. 2). This trend towards such uniquely positive
230 δ^{56}Fe values has been interpreted as due to either a decrease in oxidized meltwater discharge causing a
231 return to anoxia[16] or the shoaling of the Fe chemocline[10]; both interpretations are consistent with glacial-
232 retreat/sea-level-rise and the observed facies changes. This increasing isotopic trend corresponds with
233 increasing susceptibility, which is attributable to a rising abundance of hematite as constrained by rock
234 magnetic experiments (Fig. 5) and petrography (Fig. 6). As hematite appears to increase during periods
235 of glacial retreat and not glacial advance, this may preliminarily indicate that the O_2 is dominantly
236 supplied from polynyas during glacial minima and not meltwater discharges into tidewater during
237 glacial maxima. It should be noted, however, that assigning glacial phase relationships to orbitally forced
238 lithologic variations is difficult even for Phanerozoic climate records[26] and since both oxygenation

239 models are viable, further detailed and interdisciplinary work is required to test between their
240 contrasting climatic predictions. Either way, this strong redox gradient observed in Cryogenian BIF
241 requires both glacial advance and retreat to explain the cycles. Evidence for such dynamic, significant,
242 and sustained eustasy and/or redox variability carries several important implications for snowball Earth
243 climatology.
244
245 The observed orbital forcing reported here during the Sturtian glaciation helps resolve two fundamental
246 enigmas about snowball Earth. Firstly, widespread sedimentological variations within Cryogenian
247 diamictites were difficult to reconcile without a hydrological cycle. These features have been interpreted
248 by some as evidence against a "hard" snowball, inspiring alternative models that involved partially open
249 ocean conditions[33-36]. Documenting orbital cycles corroborates models that suggest snowball Earth ice
250 sheets were sensitive to orbital forcing[5] and accounts for well-documented Cryogenian sedimentological
251 variations and cycles[5,37] with or without partially open-ocean conditions. Secondly, molecular
252 phylogenetic clocks estimate a Sturtian origin for several crown-group metazoans[38], prompting the
253 question of how life survived snowball Earth[6,39]. Multiple refugia have been proposed[12], but the operation
254 of orbital forcing provides previously unrecognized and globally available refugia in which diversifying
255 eukaryotes could endure severe, protracted, and repeated snowball glaciations. We conclude that BIF
256 deposition during snowball glaciation and its associated episodic oxygenation of marine environments
257 were controlled by orbitally-induced advance and retreat of global ice sheets.
258

METHODS

Magnetic susceptibility

Magnetic susceptibility was measured on surface exposures of the Holowilena Ironstone using a standard-calibrated KT-10 field susceptibility metre. Cycles extracted from time series generated with such a field meter and lab-based measurements via a Kappabridge instrument have been shown to be consistent with each other[40]. Measurements were made on unique facets of a single stratigraphic horizon. Typically, ≥4 measurements were averaged at each stratigraphic level, above which precision became saturated. Field-based measurements of magnetic susceptibility allowed multiple measurements to be acquired along discrete stratigraphic layers, thereby both reducing analytical uncertainty and allowing the natural variance to be constrained. In preparation for time series analysis, long-term trends in magnetic susceptibility for each section were removed including a linear regression for Holowilena and a degree-2 polynomial for Oraparinna (Supplementary Fig. 8).

Grayscale image analysis of thin sections

Two large format (5 cm) thin sections from Holowilena were made and imaged under plane-polarized light (Supplementary Figs. 2 and 11). Photomicrographs were stitched together using the GigaPan© Software. Grayscale data were generated using the 'Plot Profile' function of the freely available ImageJ software (Supplementary Fig. 11). Pixel values were converted into stratigraphic thickness (mm) according to the length of the record selected along the thin section. In preparation for time series analysis, BIF1 (top in Supplementary Figure 11) was converted to log-scale and did not require

279 detrending, and BIF3 (bottom in Supplementary Figure 11) was detrended with a degree-3 polynomial
280 fit, which likely represents a millennial-scale cycle.
281
282 **Time series analysis**
283 We conducted time series analysis using the Fast-Fourier transform (FFT)[41] to test for the presence of
284 any significant magnetic susceptibility cycles. Spectral analyses were conducted in the stratigraphic
285 domain, which yielded a set of spectral peaks representing cycles per stratigraphic metre. For the FFT,
286 the spectral power used is the complex conjugate of the Fourier coefficients, normalized to unit mean
287 power[41]. We evaluated the significance of the FFT spectral peaks using a Monte Carlo routine to simulate
288 noise[41]. FFTs were performed on each of these 1000 randomly generated time series; a 95% confidence
289 level was approximated for each frequency by calculating three times the mean power[41]. We interpret
290 spectral peaks rising above this 95% confidence level as statistically significant, a commonly used
291 statistical threshold for identifying non-random occurrences. Based on the FFT results, we ran bandpass
292 filters with Gaussian windows to encapsulate the significant peaks identified. Amplitude modulation of a
293 bandpass, if present, was analyzed using the approach of Grippo et al.[42] in which a Hilbert transform is
294 used to find the enveloping curve of a bandpass signal (in the time domain); an FFT was performed on
295 the enveloping curve to identify the cycles of amplitude modulation of the shorter-wavelength signal.
296 Since eccentricity is rectified as climate change by its amplitude modulation of precession[1], the Hilbert
297 transform can test for evidence of such diagnostic spectral behavior.
298

299 Observed cycles in the stratigraphic domain were converted into the time domain by assuming a
300 sediment accumulation rate considered reasonable for Cryogenian strata in the Flinders Ranges (see
301 main text). Resulting observed cycle periods were then compared to target cycle periods based on
302 models of solar system evolution. Due to decelerating rotation and increasing Earth-moon distance,
303 respectively, both precession and obliquity are expected to systematically lengthen over geologic time[27]
304 (Supplementary Fig. 9; Supplementary Table 3). On the other hand, the periods for short (95 and 124
305 kyr) and long (405 kyr) eccentricity are considered constant "metronomes"[1,23]. After using the inferred
306 range of feasible sediment accumulation rates of 3.7 to 4.4 cm kyr^{-1} as an initial guideline (see main text),
307 we selected the sediment accumulation rate for each stratigraphic section that yielded the minimum net
308 misfit[43] between all observed cycles and their respective targets cycles (Supplementary Table 3).
309
310 **Rock magnetic experiments**
311 Selected samples from Oraparinna and Holowilena were ground to a fine powder. Magnetic
312 susceptibility of the samples was monitored on heating from room temperature to 700°C and subsequent
313 cooling to room temperature (at heating and cooling rates of ~11°C min^{-1}) using an AGICO KLY-4S
314 Kappabridge Susceptibility instrument. A portion of these samples were also used for room temperature
315 isothermal remanent magnetization (IRM) acquisition and hysteresis loop experiments on a Princeton
316 Measurements Corp. Model 3900 Vibrating Sample Magnetometer (VSM). IRM of the samples were
317 acquired and measured at sixty field steps on a logarithmic scale ranging from 1 mT to 1 T. Hysteresis
318 loops of the samples were measured at 5-mT field steps, with the applied field ranging between −1 T and

+1 T. Thermal susceptibility results are shown in Figure 5. All other rock magnetic experiments are summarized in Supplementary Figure 10. Oraparinna rock magnetic samples come from: BIF080, 76 m level (Fig. 2; Fig. 5a); BIF085, 71 m level (Fig. 2; Fig. 5a); BIF100, 56 m level (Fig. 2; Fig. 5a). Holowilena rock magnetic samples come from (-31.987226, 138.849969): BIF006, lower 5 metres of BIF in Holowilena logged section (Supplementary Figs. 1 and 8; Fig. 5b); HOL-1, upper 5 metres of BIF in Holowilena logged section (Supplementary Fig. 8; Fig. 5b).

Data availability

All magnetic susceptibility data are provided in Supplementary Tables 1 and 2.

Code availability

Matlab scripts used for time series analysis are available from the authors upon reasonable request.

REFERENCES

1 Hinnov, L. A. Cyclostratigraphy and its revolutionizing applications in the earth and planetary sciences. *Geological Society of America Bulletin* **125**, 1703-1734 (2013).

2 Bao, X. *et al.* Cyclostratigraphic constraints on the duration of the Datangpo Formation and the onset age of the Nantuo (Marinoan) glaciation in South China. *Earth and Planatary Science Letters* **483**, 52-63 (2018).

3 Zhang, S. *et al.* Orbital forcing of climate 1.4 billion years ago. *Proceedings of the National Academy of Sciences*, 1406-1413 (2015).

4 Lantick, M. L., Davies, J. H. F. L., Mason, P. R. D., Schaltegger, U. & Hilgen, F. J. Climate control on banded iron formations linked to orbital eccentricity. *Nature Geoscience* **12**, 369-374 (2019).

5 Benn, D. I. *et al.* Orbitally forced ice sheet fluctuations during the Marinoan Snowball Earth glaciation. *Nature Geoscience* **8**, 704-707 (2015).

6 Hoffman, P. F., Kaufman, A. J., Halverson, G. P. & Schrag, D. P. A Neoproterozoic snowball Earth. *Science* **281**, 1342-1346 (1998).

7 Partin, C. A. & Sadler, P. M. Slow net sediment accumulation sets snowball Earth apart from all younger glacial episodes. *Geology* **44**, 1019-1022 (2016).

8 Myrow, P. M., Lamb, M. P. & Ewing, R. C. Rapid sea level rise in the aftermath of a Neoproterozoic snowball Earth. *Science* **360**, 649-651 (2018).

9 Cox, G. M. *et al.* Neoproterozoic iron formation: An evaluation of its temporal, environmental and tectonic significance. *Chemical Geology* **362**, 232-249 (2013).

10 Cox, G. M. *et al.* A model for Cryogenian iron formation. *Earth and Planatary Science Letters* **433**, 280-292 (2016).

11 Le Heron, D. P., Cox, G. M., Trundley, A. & Collins, A. S. Sea ice-free conditions during the Sturtian glaciation (early Cryogenian), South Australia. *Geology* **39**, 31-34 (2011).

12 Hoffman, P. F. *et al.* Snowball Earth climate dynamics and Cryogenian geology-geobiology. *Science Advances* **3**, e1600983 (2017).

13 Lechte, M. A. & Wallace, M. W. Sedimentary and tectonic history of the Holowilena Ironstone, a Neoproterozoic iron formation in South Australia. *Sedimentary Geology* **329**, 211-224 (2015).

14 Lechte, M. A., Wallace, M. W., Hood, A. v. & Planavsky, N. J. Cryogenian iron formations in the glaciogenic Kingston Peak Formation, California. *Precambrian Research* **310**, 443-462 (2018).

15 Kirschvink, J. L. in *The Proterozoic Biosphere: A Multidisciplinary Study* (eds J.W. Schopf & C. Klein) 51-52 (Cambridge Univeristy Press, 1992).

16 Lechte, M. A. *et al.* Subglacial meltwater supported aerobic marine habitats during Snowball Earth. *Proceedings of the National Academy of Sciences* **116**, 25478-25483 (2019).

17 Reid, P. & Preiss, W. V. Parachilna map sheet. *Geological Survey of South Australia. Geological Atlas 1:250 000 Series*, sheet SH 54-13 (1999).

18 Kodama, K. P. & Hinnov, L. A. *Rock magnetic cyclostratigraphy (Vol. 5)*. (John Wiley & Sons, 2014).

19 Fairchild, I. J. *et al.* The Late Cryogenian Warm Interval, NE Svalbard: Chemostratigraphy and genesis. *Precambrian Research* **281**, 128-154 (2016).

20 Preiss, W. V. The Adelaide Geosyncline--late Proterozoic stratigraphy, sedimentation, palaeontology and tectonics. *Geological Survey South Australia Bulletin* **53**, 438 (1987).

21 Coats, R. P. COPLEY map sheet and explanatory notes, Geological Atlas of South Australia 1:250,000 series. *Geological Survey of South Australia, Australia* (1973).

22 Cox, G. M. *et al.* South Australian U-Pb (CA-ID-TIMS) age supports globally synchronous Strutian glaciation. *Precambrian Research* **315**, 257-263 (2018).

23 Hinnov, L. A. Astronomical metronome of geological consequence. *Proceedings of the National Academy of Sciences* **115**, 6104-6106 (2018).

24 Kent, D. V. *et al.* Empirical evidence for stability of the 405-kiloyear Jupiter-Venus eccentricity cycle over hundreds of millions of years. *Proceedings of the National Academy of Sciences* **115**, 6153-6158 (2018).

25 Laskar, J. *et al.* A long term numerical solution for the insolation quantities of the Earth. *Astronomy and Astrophysics* **428**, 261-285 (2004).

26 Mitchell, R. N. *et al.* Oceanic anoxic cycles? Orbital prelude to the Bonarelli Level (OAE2). *Earth and Planatary Science Letters* **267**, 1-16 (2008).

27 Berger, A. & Loutre, M. F. Astronomical forcing through geological time. *Special Publications of the International Association of Sedimentology* **19**, 15-24 (1994).

28 Waltham, D. Milankovitch period uncertainties and their impact on cyclostratigraphy. *Journal of Sedimentary Research* **85**, 990-998 (2015).

29 Meyers, S. R. & Malinverno, A. Proterozoic Milankovitch cycles and the history of the solar system. *Proceedings of the National Academy of Sciences* **115**, 6363-6368 (2018).

30 Jiang, X. & Peltier, W. R. Ten million year histories of obliquity and precession: The influence of the ice-age cycle. *Earth and Planetary Science Letters* **139**, 17-32 (1996).

31 Hrouda, F. A technique for the measurement of thermal changes of magnetic susceptibility of weakly magnetic rocks by the CS-2 apparatus and KLY-2 Kappabridge. *Geophysical Journal International* **118**, 604-612 (1994).

32 Kaplan, M. R. Retreat of a tidewater margin of the Laurentide ice sheet in eastern coastal Maine between ca. 14 000 and 13 000 14C yr B.P. *Geological Society of America Bulletin* **111**, 620-632 (1999).

33 Allen, P. A. & Etienne, J. L. Sedimentary challenge to Snowball Earth. *Nature Geoscience* **1**, 817-825 (2008).

34 Leather, J., Allen, P. A., Brasier, M. D. & Cozzi, A. Neoproterozoic snowball Earth under scrutiny: Evidence from the Fiq glaciation of Oman. *Geology* **30**, 891-894 (2002).

35 Rieu, R., Allen, P. A., Plotze, M. & Pettke, T. Climatic cycles during a Neoproterozoic "snowball" glacial epoch. *Geology* **35**, 299-302 (2007).

36 Busfield, M. E. & Le Heron, D. P. Sequencing the Sturtian icehouse: Dynamic ice behaviour in South Australia. *Journal of the Geological Society, London* **171**, 443-456 (2014).

37 Spencer, A. M. Late Pre-cambrian Glaciation in Scotland. *Geological Society, London, Memoirs* **6**, 5-102 (1971).

38 Erwin, D. H. *et al.* The Cambrian conundrum: Early divergence and later ecological success in the early history of animals. *Science* **334**, 1091-1097 (2011).

39 Runnegar, B. Loophole for snowball Earth. *Nature* **405**, 403-404 (2000).

40 Kodama, K. P. Rock magnetic cyclostratigraphy of the Carboniferous Mauch Chunk Formation, Pottsville, PA, United States. *Frontiers in Earth Science* **7**, 285 (2019).

41 Muller, R. A. & MacDonald, G. J. *Ice ages and astronomical causes: data, spectral analysis and mechanisms*. (Praxis Publishing, 2000).

42 Grippo, A., Fischer, A. G., Hinnov, L. A., Herbert, T. D. & Premoli Silva, I. in *Special Publication - Society for Sedimentary Geology, vol.81* (eds Bruno D'Argenio *et al.*) 57-81 (2004).

43 Mitchell, R. N., Kirscher, U., Kunzmann, M., Liu, Y. & Cox, G. M. Gulf of Nuna: Astrochronologic correlation of a Mesoproterozoic oceanic euxinic event. *Geology* **49**, 25-29 (2021).

44 Gernon, T. M., Hincks, T. K., Tyrell, T., Rohling, E. J. & Palmer, M. R. Snowball Earth ocean chemistry driven by extensive ridge volcanism during Rodinia breakup. *Nature Geoscience* **9**, 242-248 (2016).

ACKNOWLEDGEMENTS

We are grateful to Linda Hinnov, Paul Hoffman, Ashleigh Hood, Ken Kodama, and Bo Wan for suggestions on the manuscript. Zheng-Xiang Li supported the fieldwork with a grant from the Australian Research Council (FL150100133). Support for this work came from the National Natural Science Foundation of China (grants 41888101 and 41890833 to R.N.M), the Key Research Program of the Institute of Geology and Geophysics, Chinese Academy of Sciences (grant IGGCAS-201905 to R.N.M.), a Natural Environmental Research Council grant (NE/R004978/1 to T.M.G.), and The Alan Turing Institute (EPSRC grant EP/N510129/1 to T.M.G.). This is a contribution to International Geoscience Programme (IGCP) 648 ‘‘Supercontinent Cycles & Global Geodynamics.’’

AUTHOR CONTRIBUTIONS

R.N.M. conceived the study. R.N.M., T.M.G., G.M.C., and A.R.N. conducted the fieldwork. R.N.M. and U.K. conducted the time series analysis. Y.L. and C.X. conducted the rock magnetic experiments. R.N.M., T.M.G., X.L., and X.H., conducted the petrographic analyses. All authors contributed to the manuscript preparation, interpretation, discussion, and writing, led by R.N.M.

COMPETING INTERESTS

The authors declare no competing interests.

FIGURES

Fig. 1. Spatial and temporal distribution of banded iron formation. **a** Palaeogeographic reconstruction ca. 700 Myr ago (updated from ref. [44]) showing the locations of Cryogenian banded iron formation[9] (BIF), and hypothesized cryoconite pans (gray) where cyanobacteria and eukaryotes may have taken refuge during snowball glaciation[12]. **b** Lithologic map of the two study locations at Oraparinna and Holowilena, South Australia (updated from ref. [21]). **c** Simplified lithostratigraphy of the Sturtian glaciation in the Flinders Ranges, South Australia. **d** Fine-scale rhythmic banding observed in the Holowilena Ironstone at Holowilena.

Fig. 2. Stratigraphy, magnetic susceptibility, and δ^{56}Fe isotope geochemistry at Oraparinna. (Left) Stratigraphic log featuring the key sedimentological facies of BIF. Lower-case letters refer to outcrop

460 photographs (Supplementary Fig. 4). The colors shown, extracted from photographs, are accurate
461 representations of the rock sequence variability. The lower faulted contact is at -12 m (see
462 Supplementary Figure 5 for additional field data). (Right) Magnetic susceptibility with 2σ uncertainty
463 (black; Supplementary Table 1). δ^{56}Fe isotope variability from two sections at Oraparinna: light red is the
464 same section as ours[10], and dark red is the section of ref. [16] ~6 km along strike (Supplementary Fig. 6);
465 slightly less positive values at our section likely indicate relative proximity to the ice grounding line,
466 consistent with more stratified diamictite than in the section of ref. [16]. Best-fit degree-2 polynomials for
467 each dataset (dashed lines). Note peak values for both trends occur in the middle of the succession. Rock
468 magnetic experiments were performed on samples between 51–76 metres (Fig. 5 and Supplementary Fig.
469 10).
470
471 **Fig. 3. Time series analysis of iron formation. a** Fast-Fourier transform (FFT) of magnetic
472 susceptibility at Holowilena. Red spectra are FFT recomputed after subtracting the strongest signal (~4
473 m; ~97 kyr). Two distinct signals in the ~100 kyr bandwidth are shown as two overlapping transparent
474 dark blue bands. **b** Bandpass filters of significant cycles identified with FFT at Holowilena. Raw magnetic
475 susceptibility data are shown in gray. **c** FFT of magnetic susceptibility at Oraparinna. **d** Bandpass filters
476 of significant cycles identified with FFT at Oraparinna. Envelopes of bandpass filters exhibiting
477 amplitude modulation characterized using the Hilbert transform (Methods). Raw detrended data are
478 shown as the gray line.
479

Fig. 4. Hilbert transform of putative precession signal in order to extract putative eccentricity signal. **a** Hilbert transform (red) extracted from precession bandpass filter (blue; Fig. 3b). **b** Fast-Fourier transform (FFT) of the Hilbert transform, indicating power in the eccentricity band (compare to Figure 3a and b in the main paper), as expected.

Fig. 5. Thermal susceptibility experiments. **a** Oraparinna. Thermal susceptibility comparison between samples across a short eccentricity cycle (~100 kyr; left) and a long eccentricity cycle (~400 kyr; right). Stratigraphic heights relate to the Oraparinna section (Fig. 2). Unblocking temperatures near ~675˚C and ~585˚C indicates the presence of hematite and magnetite, respectively. Note hematite is dominant, but magnetite content is variable. Hematite-pure lithologies yield high magnetic susceptibilities and hematite-poor lithologies yield low susceptibilities. **b** Holowilena. Sample BIF006 from the lower 5 metres of the section (Supplementary Fig. 1) exhibits a dominant magnetite peak and subordinate hematite peak, whereas sample HOL-1 from the upper 5 metres contains pure hematite. Supplementary Figure 10 shows the results of other, corroborating rock magnetic experiments. Purple and red vertical bands in the background show typical ranges of (titano-)magnetite and hematite, respectively.

Fig. 6. Petrography of iron formation. **a** High susceptibility, hematite-pure hand sample (HOL-1) from Holowilena (Fig. 5b). Note red jasper is laterally discontinuous and interpreted to be chemically precipitated. **b** Photomicrographs under reflected light show randomly oriented euhedral hematite laths (white) in a quartz, chert, and clay matrix (gray). Note large gray intraclast at the bottom, also

containing hematite laths. **c** SEM images of polished thin section (top) and rock chip (bottom) exhibiting randomly oriented hematite laths in two and three dimensions, respectively. The textures strongly suggest that the hematite is authigenic (i.e., chemically precipitated) and not detrital.

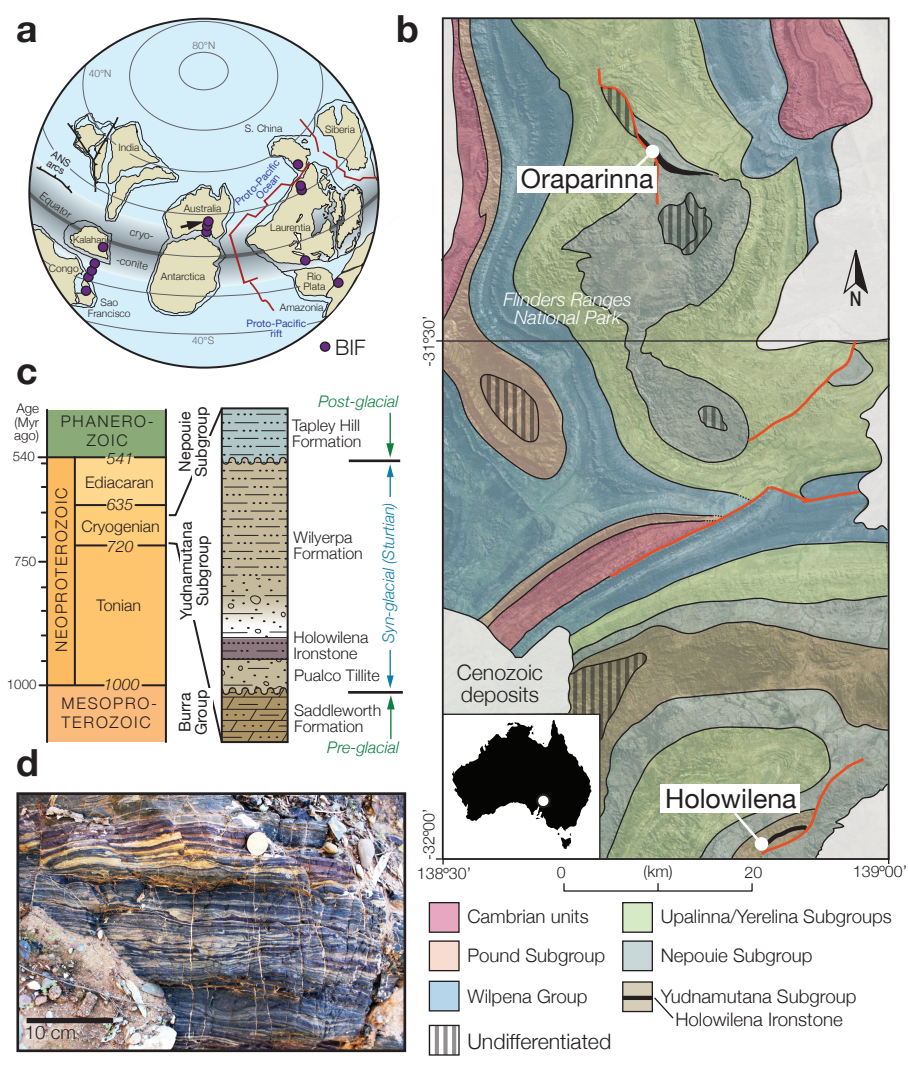
a
80°N
40°N
40°S
India
S. China
Siberia
ANS arcs
Equator
cryo-
-conite
Australia
Proto-Pacific Ocean
Laurentia
Kalahari
Congo
Antarctica
Rio Plata
Sao Francisco
Amazonia
Proto-Pacific rift
BIF
b
Oraparinna
Flinders Ranges National Park
N
-31°30'
Cenozoic deposits
Holowilena
-32°00'
138°30'
0
(km)
20
139°00'
Cambrian units
Upalinna/Yerelina Subgroups
Pound Subgroup
Nepouie Subgroup
Wilpena Group
Yudnamutana Subgroup
Holowilena Ironstone
Undifferentiated
c
Age (Myr ago)
PHANERO-ZOIC
541
Ediacaran
635
Cryogenian
720
NEOPROTEROZOIC
Tonian
1000
MESOPRO-TEROZOIC
540
750
Nepouie Subgroup
Yudnamutana Subgroup
Burra Group
Post-glacial
Tapley Hill Formation
Wilyerpa Formation
Syn-glacial (Sturtian)
Holowilena Ironstone
Pualco Tillite
Saddleworth Formation
Pre-glacial
d
10 cm

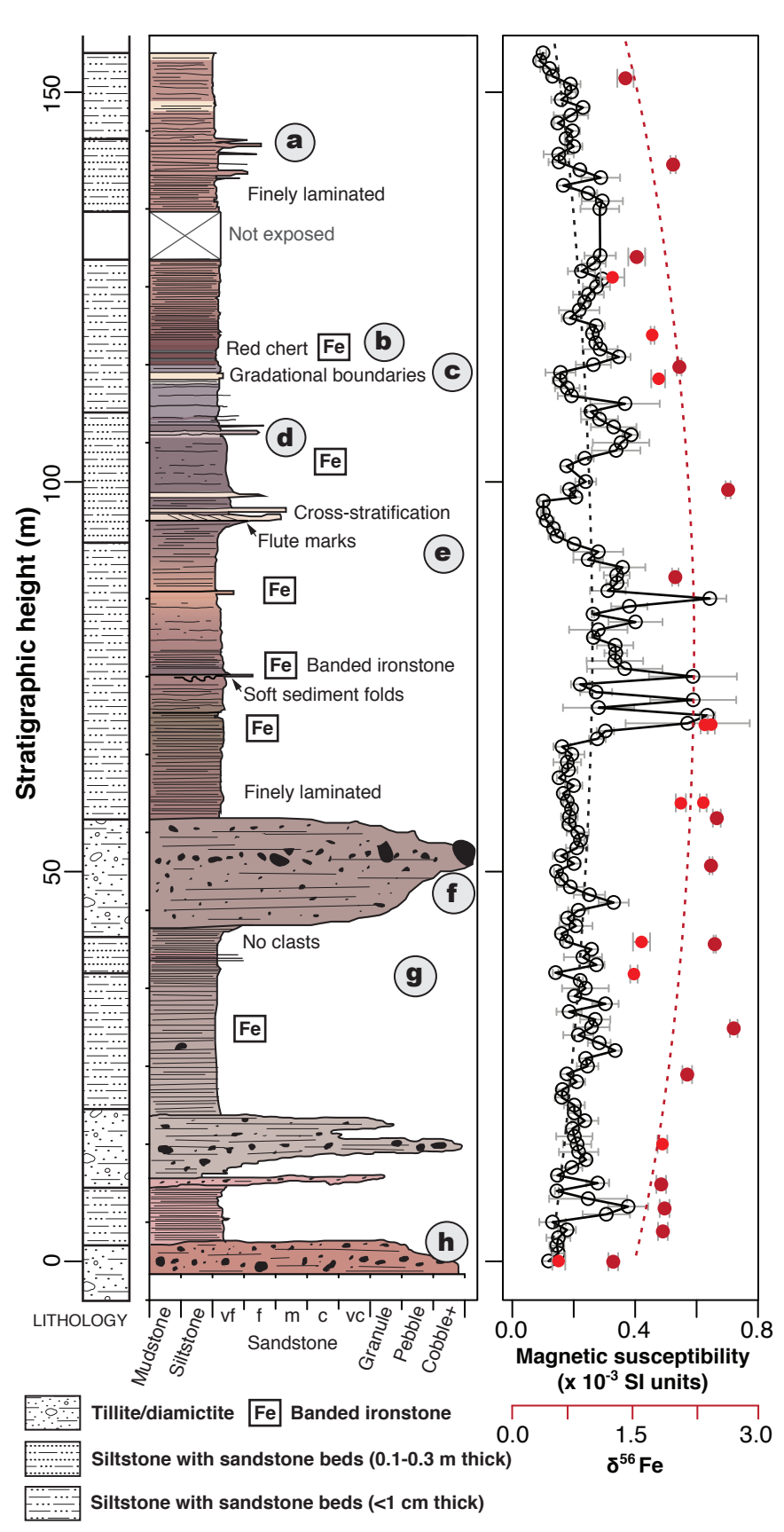
Stratigraphic height (m)
150
100
50
0
a
Finely laminated
Not exposed
Red chert
Fe
b
Gradational boundaries
c
d
Fe
Cross-stratification
Flute marks
e
Fe
Fe
Banded ironstone
Soft sediment folds
Fe
Finely laminated
f
No clasts
g
Fe
h
LITHOLOGY
Mudstone
Siltstone
vf
f
m
c
vc
Sandstone
Granule
Pebble
Cobble+
0.0
0.4
0.8
Magnetic susceptibility
(x 10-3 SI units)
Tillite/diamictite
Fe
Banded ironstone
Siltstone with sandstone beds (0.1-0.3 m thick)
Siltstone with sandstone beds (<1 cm thick)
0.0
1.5
3.0
δ56 Fe

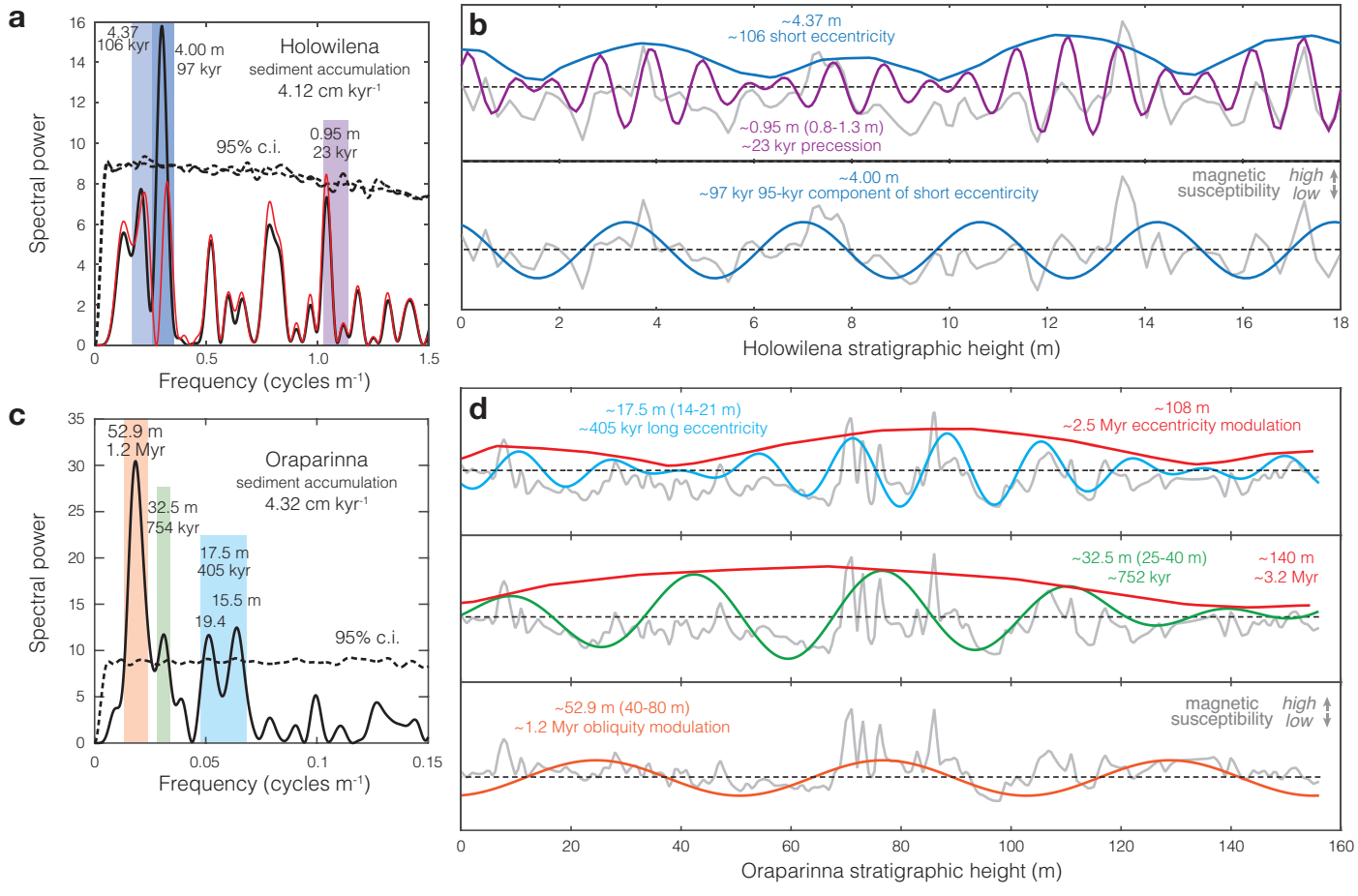
a
4.37
106 kyr
4.00 m
97 kyr
Holowilena
sediment accumulation
4.12 cm kyr-1
95% c.i.
0.95 m
23 kyr
Spectral power
Frequency (cycles m-1)
b
~4.37 m
~106 short eccentricity
~0.95 m (0.8-1.3 m)
~23 kyr precession
~4.00 m
~97 kyr 95-kyr component of short eccentricity
magnetic susceptibility
high
low
Holowilena stratigraphic height (m)
c
52.9 m
1.2 Myr
32.5 m
754 kyr
17.5 m
405 kyr
15.5 m
19.4
Oraparinna
sediment accumulation
4.32 cm kyr-1
95% c.i.
Spectral power
Frequency (cycles m-1)
d
~17.5 m (14-21 m)
~405 kyr long eccentricity
~108 m
~2.5 Myr eccentricity modulation
~32.5 m (25-40 m)
~752 kyr
~140 m
~3.2 Myr
~52.9 m (40-80 m)
~1.2 Myr obliquity modulation
magnetic susceptibility
high
low
Oraparinna stratigraphic height (m)

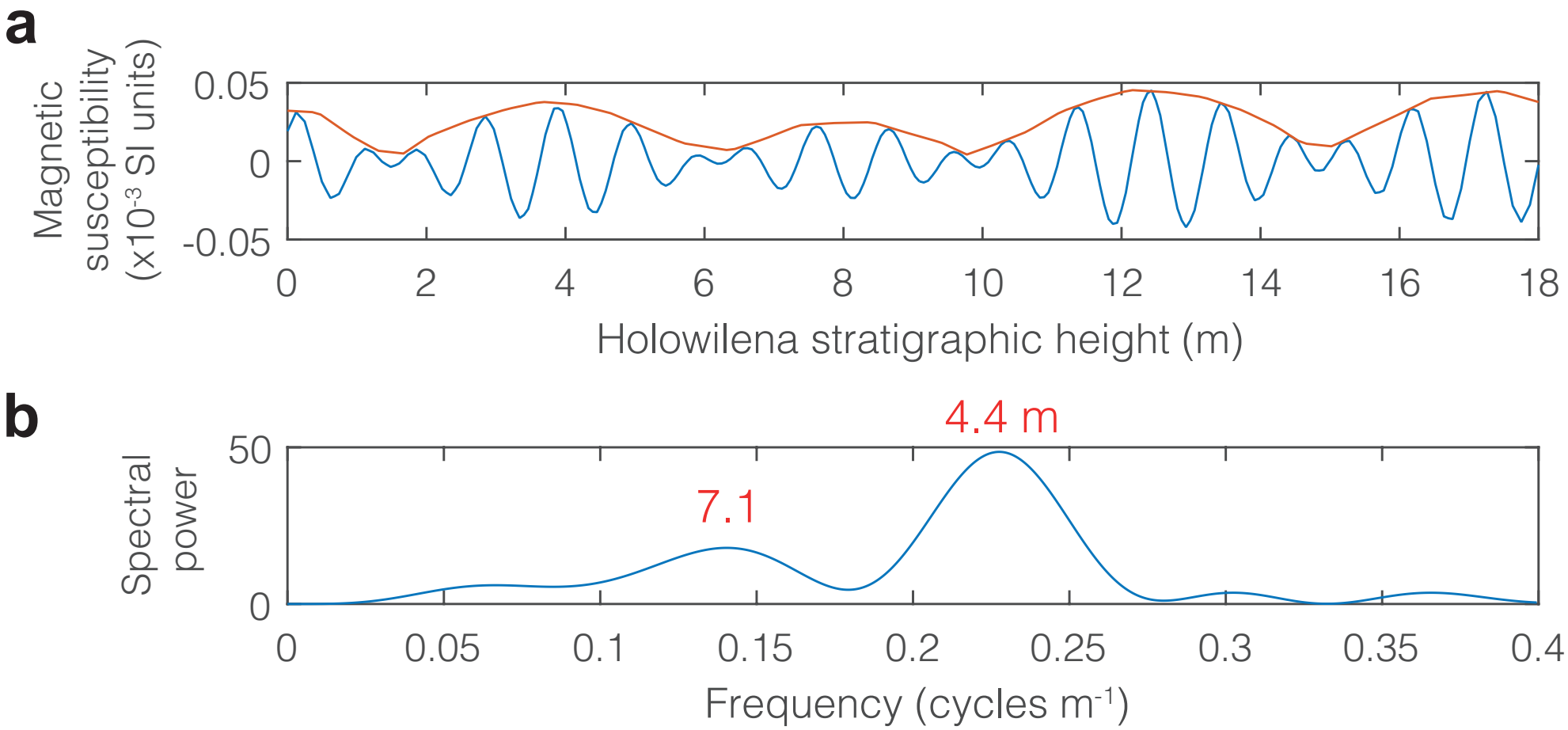
a
Magnetic susceptibility (x10-3 SI units)
0.05
0
-0.05
0
2
4
6
8
10
12
14
16
18
Holowilena stratigraphic height (m)
b
Spectral power
50
0
4.4 m
7.1
0
0.05
0.1
0.15
0.2
0.25
0.3
0.35
0.4
Frequency (cycles m-1)

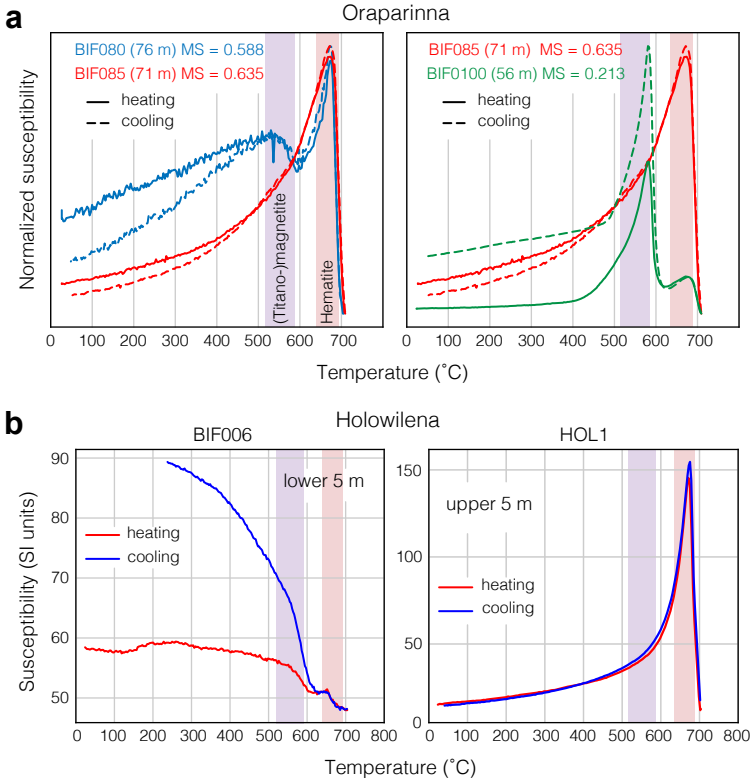
a
Oraparinna
BIF080 (76 m) MS = 0.588
BIF085 (71 m) MS = 0.635
heating
cooling
(Titano-)magnetite
Hematite
BIF085 (71 m) MS = 0.635
BIF0100 (56 m) MS = 0.213
heating
cooling
Normalized susceptibility
0 100 200 300 400 500 600 700
0 100 200 300 400 500 600 700
Temperature (°C)
b
Holowilena
BIF006
lower 5 m
heating
cooling
HOL1
upper 5 m
heating
cooling
Susceptibility (SI units)
90 80 70 60 50
150 100 50 0
0 100 200 300 400 500 600 700 800
0 100 200 300 400 500 600 700 800
Temperature (°C)

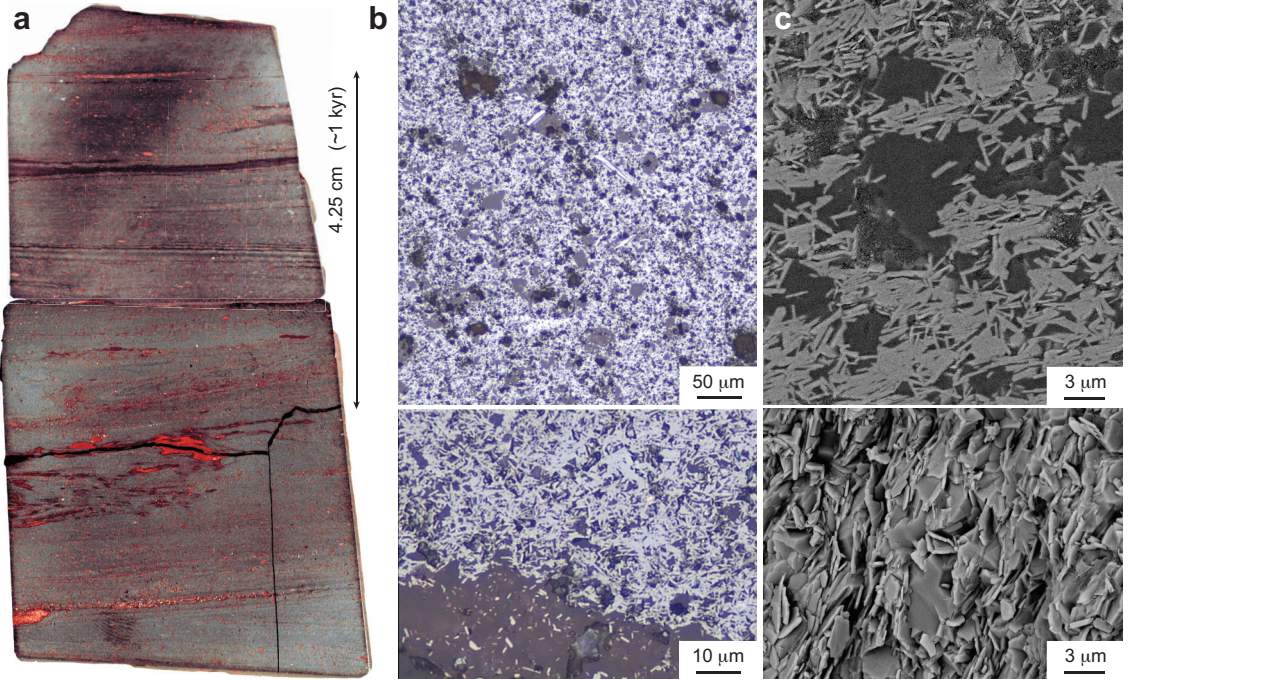
a
4.25 cm
(~1 kyr)
b
50 μm
10 μm
c
3 μm
3 μm